A Fuzzy Regional-Based Approach
for Detecting Cerebrospinal Fluid Regions
in Presence of Multiple Sclerosis Lesions

Francesc Xavier Aymerich[1,2], Eduard Montseny[2], Pilar Sobrevilla[3], and Alex Rovira[1]

[1] Unitat RM Vall Hebron (IDI). Hospital Vall Hebron, 08035 Barcelona, Spain
{xavier.aymerich,alex.rovira}@idi-cat.org
[2] ESAII Departament, Universitat Politècnica de Catalunya, 08034, Barcelona, Spain
{xavier.aymerich,eduard.montseny}@upc.edu
[3] MAII Departament, Universitat Politècnica de Catalunya, 08034, Barcelona, Spain
pilar.sobrevilla@upc.edu

Abstract. Magnetic Resonance Imaging (MRI) is an important paraclinical tool for diagnosing and following-up of Multiple Sclerosis (MS). The detection of MS lesions in MRI may require complementary information to filter false detections. Given that MS lesions cannot be located within cerebrospinal fluid (CSF), detection of this region is very helpful for our purpose. Although T1-weighted images are usually chosen to detect CSF regions, the gray level similarity between some MS lesions and CSF regions difficult this task. With the aim of discriminating CSF region within intracranial region, but considering aforementioned drawback, we propose a fuzzy-based algorithm that involves the regional analysis of the fuzzy information obtained from a previous local analysis. The proposed algorithm introduces location, shape and size constraints in CSF detection, and provides confidence degrees associated with the possibility of including MS lesion pixels.

Keywords: Magnetic resonance imaging, brain, multiple sclerosis, cerebrospinal fluid, fuzzy sets, regional analysis.

1 Introduction

Multiple sclerosis (MS) is a disease of the central nervous system (CNS) characterized by the destruction of the myelin that encases the axons. This demyelinating process results in an inhibition of neural transmission and causes the appearance of several clinical symptoms, such as motor and sensory disturbances, paralysis or visual alterations [1]. The diagnosis and follow-up of this disease involves the use magnetic resonance imaging (MRI), which is recognized as the imaging method of choice for examination of CNS disorders [2]. In the study of MS, MRI also plays a relevant role as diagnostic criteria [3][4].

Among all the different weighted images that can be obtained by MRI, T1-weighted images are the preferred choice for the analysis of the intracranial region. This is due to its high degree of anatomic information, and because they show good contrast between the parenchyma region and the cerebrospinal fluid (CSF) [5].

Although several algorithms have been proposed for the analysis of the intracranial region in T1-weighted images, most of them are focused on segmentation considering healthy volunteers [6][7] or other pathologies [7][8]. Consequently, these methods do not take into account the problems that the presence of MS lesions can introduce in the segmentation process.

In MS patients, the analysis of the intracranial region considering T1-weighted images is focused on tasks such as the measurement of brain volumes [9], the evaluation of black holes [10], and filtering false detections. Most of these tasks require the differentiation of the encephalic parenchyma in relation of its environment to achieve an accurate segmentation. In spin-echo or gradient-echo T1-weighted images, the similarity of gray-level values between CSF and MS hypointense lesions can introduce misclassifications of MS lesions as CSF instead of as parenchyma [11].

Recently we proposed an algorithm [12] for detecting CSF regions in presence of MS lesions considering a single T1-weighted scan. This algorithm carried out a local fuzzy analysis based on gray-level and texture features associated with CSF regions that allowed representing the intrinsic vagueness of the CSF features. However we observed the necessity of introducing a further analysis to take into consideration some location, shape and size constraints that the local analysis could not include. So, in this work we propose a regional fuzzy-based algorithm that allows taking into account aforementioned constraints. The use of fuzzy techniques will allow dealing with the vagueness of the CSF features, and will provide confidence degrees associated with the possibility that detections could correspond to MS lesions.

2   Definition of the CSF Regions

We considered axial slices acquired in a Siemens 1.5T Magnetom Vision MR System (Erlangen, Germany) using a T1-weighted spin-echo sequence (TR/TE/NEX/FA 667ms/14ms/1/70°) to cover a field of view of 250 mm in each 3 mm slice.

Based on the analysis of the anatomical structures of these images, in [12] we observed that CSF regions, such as the sulci or the ventricular regions, can be divided according to its width as follows:

1. Wide CSF regions (**WFR**): fluid regions whose width is equal to or greater than 5 pixels.
2. Narrow CSF regions (**NFR**): fluid regions whose width is lower than 5 pixels.

Due to MS lesions contiguous to CSF may be difficult to differentiate from CSF regions, we also differentiated inner and peripheral wide and narrow CSF regions. These regions were described based on gray level and texture features as follows:

1.1 Inner Wide Fluid Region (**IWFR**): region whose pixels show dark gray level –*dwgl*- and homogeneous texture –*ht*-.
1.2 Peripheral Wide Fluid Region (**PWFR**): region whose pixels show medium-dark gray level –*mdgl*- and micro-grainy texture –*mgt*-.
2.1 Inner Narrow Fluid Region (**INFR**): region whose pixels show dark gray level –*dngl*- and very micro-grainy texture –*vmgt*-.
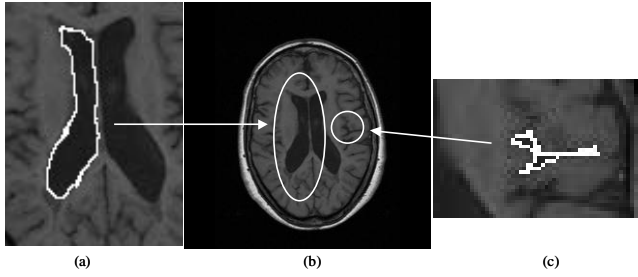
Fig. 1. Detail of the different CSF regions considered. (b) is the original image, (a) is a zoomed area that shows IWFR dark region surrounded by PWFR (solid white line), and (c) shows a zoomed area of the INFR dark regions surrounded by PNFR (solid white line).

2.2 Peripheral Narrow Fluid Region (**PNFR**): region whose pixels show medium-dark gray level –*mdgl*- and very micro-grainy texture –*vmgt*-.

Figure 1 depicts the locations of the regions above described. Image (a) shows that PWFR surround IWFR, whereas having a look at image (c) it can be appreciated that pixels in narrow regions labeled as PNFR do not require the proximity of INFR.

3 Local Analysis within Intracranial Region

Local analysis involved the study of perceptual features, gray level and texture, within intracranial region. This study required of two preprocessing tasks: Extraction of the intracranial region using a previously developed algorithm [13]; and normalization of the gray-level values to increase the gray-level uniformity among different slices.

Given the vagueness associated with the considered perceptual features, the local analysis carried out in [12] was based on the definition of the fuzzy sets F_{IWFR}, F_{PWFR}, F_{INFR} and F_{PNFR} associated with the four regions introduced at previous section, which were obtained aggregating the antecedent fuzzy sets –F_{dngl}, F_{dwgl}, F_{mdgl}, F_{vgt}, F_{gt} and F_{ht}- associated with the perceptual features *dngl*, *dwgl*, *mdgl*, *vgt*, *gt* and *ht* as follows:

$$\mu_{IWFR}(p_{ij}) = 0.7\, \mu_{dwgl}(p_{ij}) + 0.3\, \mu_{ht}(p_{ij}); \quad \mu_{PWFR}(p_{ij}) = 0.8\, \mu_{mdgl}(p_{ij}) + 0.2\, \mu_{gt}(p_{ij}). \tag{1}$$

$$\mu_{PWFR}(p_{ij}) = 0.8\, \mu_{mdgl}(p_{ij}) + 0.2\, \mu_{gt}(p_{ij}); \quad \mu_{PNFR}(p_{ij}) = \min(\mu_{mdgl}(p_{ij}), \mu_{vgt}(p_{ij})). \tag{2}$$

Where μ_{dngl} and μ_{mdgl} were obtained through the evaluation of the normalized gray levels; μ_{dwgl} by assigning the mean gray level of pixels inside a 3x3 raster window to the central pixel; and texture membership functions, μ_{ht}, μ_{vgt}, and μ_{gt}, were obtained analyzing the differences among the gray levels of the central and surrounding pixels within square raster windows of size 3x3 for ht, 7x7 in the cases of vgt and gt.

4 Algorithm and Methodology

As we are interested in detecting CSF region within images containing MS lesions, the proposed algorithm takes into account CSF regional constraints to improve the

results obtained by previously described local analysis. So, regional analysis consisted of obtaining new membership functions related to the fuzzy sets F_{IWFR}, F_{PWFR}, F_{INFR} and F_{PNFR} by considering the regional constraints of the regions given in section 2.

4.1 Obtaining Improved IWFR Membership Function

Analyzing the outcomes of local algorithm, it was appreciated that some IWFR pixels had low μ_{IWFR} values due to noise or image non-homogeneity. To avoid this problem it was considered that: "*A pixel p_{ij} is IWFR if it is surrounded by pixels of IWFR, although there can be some very small neighboring regions that are not IWFR*".

Given the characteristics of IWF regions, to implement previous property we considered four masks: A circular mask of 1.5 pixel radius, M_1; a circular ring, M_2, with radii 1.5 and 2.5 pixels; a circular ring, M_3, with inner and outer radii 1.5 and 3.2 pixels, divided into four regions ($\{M_3^k\}_{k=1}^4$), each having 7 pixels; and a circular mask, M_4, of 3.2 pixel radius divided into 4 inner regions ($\{M_{4I}^k\}_{k=1}^4$), with 2 pixels each, and 4 outer regions ($\{M_{4O}^k\}_{k=1}^4$) that match the ones of previous mask.

Then, once mask M_k is centered on pixel p_{ij}, $\mu_{M_k}(p_{ij})$ is obtained aggregating the membership values of the pixels covered by M_k using OWA operators [14] as follows:

-   $W_{M_1} = (0,0,0,0,1,0,0,0)$ and $W_{M_2} = (0,0,0,0,0,0,0,0,0,1,0,0)$ are the weighting vectors applied for getting $\mu_{M_1}(p_{ij})$ and $\mu_{M_2}(p_{ij})$ respectively.

-   Weighting vector $W_{M_3^k} = (0,0,0,0,0,1,0)$ are the used for obtaining the membership values $\mu_{M_3^k}(p_{ij})$ ($1 \leq k \leq 4$). Then, these values are aggregated by using $W_{M_3} = (0,0,1,0)$ for obtaining $\mu_{M_3}(p_{ij})$.

-   $W_{M_{4I}^k} = (0,1)$ and $W_{M_{4O}^k} = (0,0,0,0,0,1,0)$ are the weighting vectors applied for getting $\mu_{M_{4I}^k}(p_{ij})$ and $\mu_{M_{4O}^k}(p_{ij})$. Then, for each k ($1 \leq k \leq 4$), we get $\mu_{M_4^k}(p_{ij})$ using $W_{M_4^k} = (0,1)$, and finally these values are aggregated by using $W_{M_4} = (0,0,1,0)$ for obtaining $\mu_{M_4}(p_{ij})$.

Then, the improved fuzzy set F_{IWFR} is given by the membership function:

$$\eta_{IWFR}(p_{ij}) = \begin{cases} \mu_{IWFR}(p_{ij}) & if \quad \mu_{IWFR}(p_{ij}) > 0.75 \\ \max(\mu_{M_1}(p_{ij}), \mu_{M_2}(p_{ij}), \mu_{M_3}(p_{ij}), \mu_{M_4}(p_{ij})) & otherwise \end{cases}. \quad (3)$$

4.2 Obtaining Improved PWFR Membership Function

Regionally, a PWFR is a thin and closed region surrounding a IWF region. So, to improve the outcomes of local algorithm, we first considered the contiguity of PWFR and IWFR. To do it, for each pixel p_{ij} the membership values, $\mu_{IWFR}(p_{kl})$, of the pixels p_{kl} covered by a circular mask of 2 pixel radius (M_5), centered in p_{ij}, were aggregated using an OWA operator of weighting vector $W_5 = (0,1,0,0,0,0,0,0,0,0,0,0)$. In this way

we obtained a new membership value $\mu_{M_5}(p_{ij})$, that was used for getting the improved PWFR membership function given by equation (4).

The values of the parameters in this equation were obtained taking into account that a pixel of PWFR must show a *high enough* membership degree to F_{PWFR}, and F_{IWFR} in its neighborhood. Since a pixel of PWFR requires the presence of a minimum number of pixels belonging to IWFR in its near neighborhood showing high μ_{IWFR} value, we gave more relevance to the parameter associated with $\mu_{M_5}(p_{ij})$. Then, we obtained the values by heuristic analysis of the PWFR region at different locations. (An analogous process was applied for obtaining the parameters of next equations.)

$$\mu_{PFWR}(p_{ij}) = \begin{cases} 0.15\mu_{PWFR}(p_{ij}) + 0.85\mu_{M_5}(p_{ij}) & \text{if } \mu_{PWFR}(p_{ij}) > 0.4 \\ \mu_{PWFR}(p_{ij}) & \text{otherwise} \end{cases}. \quad (4)$$

Analyzing the results of the local algorithm, it was observed that the values of μ_{PWFR} and μ_{IWFR} were too low for some pixels adjacent to IWFR. To overcome this drawback we applied a morphological dilation -δ_{c1}- to previous values using a circular structuring element of radius 1. Then, the improved membership function defining F_{PWFR} is given by equation (5), where δ_{c1}^{IWFR} and δ_{c1}^{PWFR} are the values obtained by applying δ_{c1} on the values given by μ_{IWFR} and μ_{PWFR}, respectively.

$$\eta_{PFWR}(p_{ij}) = \begin{cases} \max(\mu_{PWFR}^I(p_{ij}), \delta_{c1}^{IWFR}(p_{ij})) & \text{if } \delta_{c1}^{IWFR}(p_{ij}) > 0.5 \\ \min(1-\eta_{IWFR}(p_{ij}), \delta_{c1}^{IWFR}(p_{ij})) & \text{if } \{\min(\delta_{c1}^{IWFR}(p_{ij}), \delta_{c1}^{PWFR}(p_{ij})) > 0.5 \text{ and } \mu_{PWFR}^I(p_{ij}) \le 0.5\} \\ \mu_{PWFR}^I(p_{ij}) & \text{otherwise} \end{cases}. \quad (5)$$

4.3 Obtaining Improved INFR Membership Function

Because of pixels within Inner Narrow Fluid regions can not be connected with central locations of wide fluid regions, to improve the outcomes of local algorithm we considered that: "*If pixel p_{ij} is INFR and is connected to any pixel that is PWFR or IWFR in a central location of the intracranial region, then p_{ij} is not INFR*".

To implement the central location property, given the set R_{cent} that contains the 60% of more inner pixels within the intracranial region, we defined the membership function $\mu_{WCR}(p_{ij})$ as equal to the maximum of $\eta_{IWFR}(p_{ij})$ and $\eta_{PWFR}(p_{ij})$ for all the pixels of R_{cent}, and equal to zero otherwise. For implementing the connectivity we considered the binary image I_B such that $I_B(i,j)=1$ if $\max(\mu_{WCR}(p_{ij}), \mu_{INFR}(p_{ij}))>0.5$, and $I_B(i,j)=0$ otherwise. Then, if $C(p_{ij})$ is the set of pixels 8-connected to p_{ij} in I_B, we define $mwr(p_{ij})$ as the mean value of μ_{WCR} evaluated on $C(p_{ij})$. Moreover we considered the connectivity function $CF(p_{ij}, \mu_{WCR}, 0.5)$ that counts the number of pixels within a 8-neighborhood of p_{ij}, whose values in μ_{WCR} are greater than 0.5. Using these expressions the improved membership function is given by:

$$\eta_{INFR}(p_{ij}) = \begin{cases} \min(\mu_{INFR}(p_{ij}), 1-mwr(p_{ij})) & \text{if } \{\mu_{INFR}(p_{ij}) > 0.5 \text{ and } CF(p_{ij}, \mu_{WCR}, 0.5) > 0\} \\ \mu_{INFR} & \text{otherwise} \end{cases}. \quad (6)$$

4.4 Obtaining Improved PNFR Membership Function

As a result of improvements on INFR, we need to review the peripheral narrow fluid regions in the proximity of pixels where $\eta_{INFR}(p_{ij}) < \mu_{INFR}(p_{ij})$. Thus, being p_{ij} a pixel whose $\mu_{PNFR}(p_{ij})$ shows a high enough membership degree but there exist a pixel p_{kl} within a 3x3 raster window centered on p_{ij} such that $\eta_{INFR}(p_{kl}) < \mu_{INFR}(p_{kl})$, then p_{ij} may not be PNFR. To do it, we applied the following expression:

$$\eta_{PNFR} = \begin{cases} \min(\eta_{INFR}(p_{ij}), \mu_{PNFR}(p_{ij})) & if \quad \mu_{PNFR}(p_{ij}) > 0.5 \ and \ CF(p_{ij}, \mu_{INFR} - \eta_{INFR}, 0) > 0 \\ \mu_{PNFR}(p_{ij}) & otherwise \end{cases}. \tag{7}$$

4.5 Introduction of Confidence Degrees in the Detection

Since misclassification of MS lesion pixels as CSF pixels highly depends on pixel location, we considered that *exists confidence* in the detection of a pixel as CSF if it presents a low possibility of misclassification as MS lesion pixel based on its location.

The definition of *confidence* was based on the aggregation of the fuzzy sets F_{PWFR}, F_{IWFR}, F_{PNFR} and F_{INFR} considering location and size constraints of the regions involved, and the possibility that lesion is present at them. Taking into account that narrow and wide fluid regions have different regional characteristics, we defined four new fuzzy sets: F_{CNFR}, and F_{CWFR}, which provide the possibility of a pixel to be detected as CSF in areas of narrow and wide fluid regions where there exists confidence in the detection; and F_{NCNFR} and F_{NCWFR} that are associated with areas in which there exists a higher possibility of misclassification. The membership functions that define F_{CNFR} and F_{NCNFR} are given by:

$$\mu_{CNFR}(p_{ij}) = \begin{cases} \min(\max(\eta_{PNFR}(p_{ij}), \eta_{INFR}(p_{ij})), \mu_{MPNFR}(p_{ij})) \\ \qquad\qquad if \quad \begin{cases} CF(p_{ij}, \eta_{INFR}, 0.5) > 0 \quad and \\ \max(\eta_{PNFR}(p_{ij}), \eta_{INFR}(p_{ij})) > 0.5 \end{cases} \\ \min(\eta_{PNFR}(p_{ij}), \eta_{INFR}(p_{ij}), \mu_{MPNFR}(p_{ij})) \qquad otherwise \end{cases}. \tag{8}$$

$$\mu_{NCNFR} = \min(\max(\eta_{PNFR}, \eta_{INFR}), 1 - \mu_{CNFR}). \tag{9}$$

where $\mu_{MPNFR}(p_{ij}) = \max(\mu_{PNFR}(p_{ij}), \mu_{INFR}(p_{ij}))$ if p_{ij} belongs to a region, R, whose pixels satisfy that $\max(\mu_{PNFR}(\bullet), \mu_{INFR}(\bullet)) > 0.5$, and at least a 60% of the pixels within R are in the 20% most outer pixels of the intracranial region; and, $\mu_{MPNFR}(p_{ij}) = 0$ otherwise.

As previously said, unlike narrow fluid regions, in wide CSF regions the higher possibility of correct detection is based on size constraints. Thus, if I_{WFR} is the binary image such that $I_{WFR}(i,j) = 1$ if p_{ij} belongs to a region with a minimum width of 5 pixels whose pixels satisfy that $\max(\eta_{PWFR}(p_{ij}), \eta_{PNFR}(p_{ij})) > 0.5$, and $I_B(i,j) = 0$ otherwise. Then, the membership functions defining F_{CWFR} and F_{NCWFR} are given by:

$$\mu_{CWFR} = \begin{cases} 0.4 & if \quad \eta_{IWFR}(i,j) > 0.5 \ and \ I_{WFR}(i,j) = 0 \\ \eta_{IWFR} & otherwise \end{cases}. \tag{10}$$

$$\mu_{NCWFR} = \begin{cases} 0.2 & if \quad \eta_{IWFR}(i,j) > 0.5 \quad and \quad I_{WFR}(i,j) = 1 \\ \eta_{PWFR} & otherwise \end{cases} . \tag{11}$$

Finally, the degrees of confidence and no confidence in the detection were given by aggregation of previous membership functions according following expressions:

$$\mu_{CFR}(p_{ij}) = \begin{cases} 0.5 & if \begin{cases} (\max(\mu_{CWFR}(p_{ij}),\mu_{CNFR}(p_{ij})) > 0.5) \ and \\ (\max(\mu_{NCWFR}(p_{ij}),\mu_{NCNFR}(p_{ij})) > 0.5) \ and \\ (\max(\mu_{CWFR}(p_{ij}),\mu_{CNFR}(p_{ij})) \leq \\ \qquad \max(\mu_{NCWFR}(p_{ij}),\mu_{NCNFR}(p_{ij})) - 0.1) \end{cases} \\ \max(\mu_{CWFR}(p_{ij}),\mu_{CNFR}(p_{ij})) \qquad otherwise \end{cases} . \tag{12}$$

$$\mu_{NCFR}(p_{ij}) = \begin{cases} 0.5 & if \begin{cases} (\max(\mu_{CWFR}(p_{ij}),\mu_{CNFR}(p_{ij})) > 0.5) \ and \\ (\max(\mu_{NCWFR}(p_{ij}),\mu_{NCNFR}(p_{ij})) > 0,5) \ and \\ (\max(\mu_{CWFR}(p_{ij}),\mu_{CNFR}(p_{ij})) > \\ \qquad \max(\mu_{NCWFR}(p_{ij}),\mu_{NCNFR}(p_{ij})) - 0.1) \end{cases} \\ \max(\mu_{NCWFR}(p_{ij}),\mu_{NCNFR}(p_{ij})) \qquad otherwise \end{cases} . \tag{13}$$

4.6　Defuzzification and Quality Measures

The defuzzification process focused on obtaining the CSF region applying α-cuts to CFR and NCFR fuzzy sets. Then, the crisp representation of the CSF was obtained adding the binary results obtained for CFR and NCFR.

To determine the appropriate α-cuts we defined a detection quality factor, Q_{DFR}, obtained evaluating the efficiency in the detection of CSF regions, E_{FRP}, and considering two reliability factors: R_{FRP}, related to the number of CSF pixels detected; related to the number of MS lesion pixels. So, if N_{DFRP} is the number of detected CSF pixels, N_{NDFRP} is the number of non-detected CSF pixels, N_{FDFR} is the number of false detections detecting CSF pixels, N_{DLP} is the number of detected MS lesion pixels, and N_{LP} is the total number of MS lesion pixels, the efficiency in the detection and the reliability factors were defined by equations (14) and (15). Then the quality factor, Q_{DFR}, is given by equation (16).

$$E_{FRP} = 2\frac{N_{DFRP}}{2N_{DFRP} + N_{NDFRP} + N_{FDFR}} . \tag{14}$$

$$R_{FRP} = \frac{N_{DFRP}}{N_{DFRP} + N_{NDFRP}} ; \quad R_{NDLP} = 1 - \frac{N_{DLP}}{N_{LP}} . \tag{15}$$

$$Q_{DFR} = 0.6\left(\frac{E_{FRP} + R_{FRP}}{2}\right) + 0.4R_{NDLP} . \tag{16}$$

CSF and MS lesion masks were manually obtained using Dispimage software [15].

The α-cuts had to provide a commitment between correct detection of fluid regions and avoiding misclassification. So for selecting the more suitable we studied the results obtained for α-cuts in the interval [0.55, 0.95] for the training images.

5   Results

The proposed algorithm was evaluated considering a training set compounded by 6 images acquired from two patients, and a test set constituted by 138 images acquired from three patients. All images were acquired using the T1-weighted sequence described in section 2.

From the study of the results obtained applying nine α-cuts in the interval [0.55, 0.95] to the values of μ_{CFR} for the training images, we selected the value 0.55 because it provided the higher CFR quality detection outputs, without misclassifications as MS lesions. Then, we considered the union of the binary image obtained applying this á-cut to μ_{CFR} and the binary images obtained applying the nine α-cuts to μ_{NCFR}. Next, we obtained their quality indexes, Q_{DFR}, and analyzing the results we observed that the optimal value was gotten when the α-cut for μ_{NCFR} was 0.55.

Having a look at columns 3 and 4 of Table 1, it can be appreciated that the indexes related to detection of CSF pixels, E_{FRP} and R_{FRP}, obtained considering the union improved the results obtained for the CFR, whereas we detected a reduced number of MS pixels. Moreover, looking at column 6 of Table 1 can be appreciated that global quality Q_{DFR} achieved an improvement around of 10% when NCFR is considered.

It must be pointed out that the introduction of regional analysis represented a significant improvement of the results over local analysis in the CFR, because E_{FRP} and R_{FRP} quality indexes increased around of 10-16%. In the case of R_{NDLP} and Q_{DFR} quality indexes, their values kept in the same range with absence of misclassifications and a slight better Q_{DFR} in the regional analysis.

The results obtained for the test images are shown at Table 2. As can be appreciated, the values of all quality factors obtained for the regional analysis (rows 2 and 4) improved the obtained with local analysis (rows 3 and 5). Differences in relation to

Table 1. Quality results obtained considering the training set images after regional analysis

Region	α-cut	E_{FRP}	R_{FRP}	R_{NDLP}	Q_{DFR}
CFR	0.55	0.673	0.580	1.0	0.776
CFR∪NCFR	0.55	0.724	0.832	0.951	0.847

Table 2. Summary of quality results obtained for CFR∪NCFR considering the test set images after regional analysis

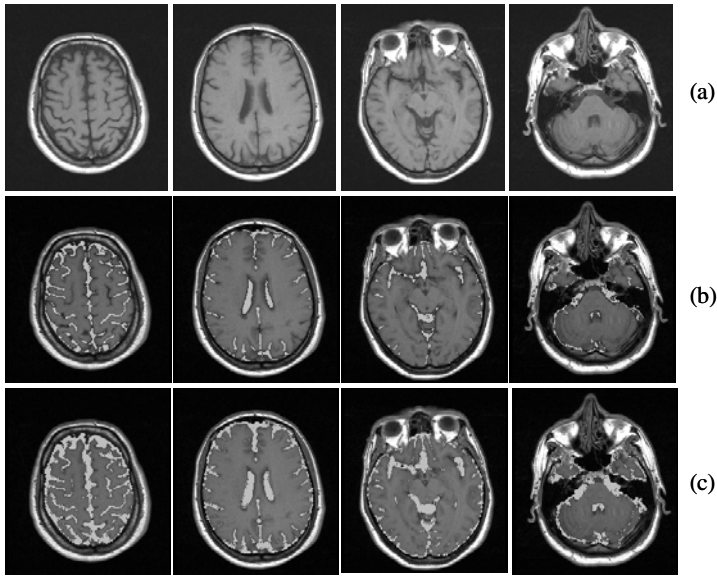| Region		E_{FRP}	R_{FRP}	R_{NDLP}	Q_{DFR}
CFR	Regional	0.557	0.430	0.999	0.696
	Local	0.469	0.338	0.999	0.642
CFR∪NCFR	Regional	0.726	0.708	0.925	0.800
	Local	0.696	0.651	0.886	0.758

Fig. 2. Different levels of detection corresponding to different anatomical locations. (a) Original images. (b) Detection mask corresponding to CFR overlaid on the original images. (c) Detection mask corresponding to CFR∪NCFR overlaid on the original images.

the analysis of the images included in the training set showed, mainly, a reduction of CSF detection for CFR, whereas the capability of avoiding misclassifications was very close to the obtained for the training set. These results can be appreciated in Fig. 3 that shows some examples of results in the analysis of the test set corresponding to different anatomical locations.

To conclude, in this paper we have presented an algorithm which allows discriminating cerebrospinal fluid regions inside the intracranial region, providing confidence degrees that match with the possibility of including pixels associated to MS lesions. This work has focused on the introduction of a regional analysis in order to improve detections levels obtained after local analysis based on perceptual features. Thereby, the proposed algorithm has considered location, shape and size constraints, and has divided the results in function of the level of confidence in avoiding misclassification of MS pixels as CSF detections. The results show good CSF detection levels, and the values of the quality factors point out that CFR is free or practically free of misclassifications, whereas NCFR helped to improve CSF detection level without increasing significantly the number of misclassifications. The introduction of regional analysis has allowed improving both CSF detection levels and confidence in avoiding misclassifications in relation to previous local analysis. It must be also emphasized the improvements in values of R_{NDLP} quality factors and in the quality levels obtained considering the test set. Finally, the results obtained suggest that this algorithm, particularly images resulting of detecting CFR regions, can be applied to filter false detections of MS lesions due to misclassifications of these lesions as CSF. An improvement of the work here presented may be the introduction of an alternative approach to obtain the values of the parameters based on an optimization procedure; which would also help to carry out a robustness study.

References

1. Edwards, M.K., Bonnin, J.M.: White Matter Diseases in Magnetic Resonance Imaging of the Brain and Spine. In: Atlas, S.W. (ed.) Magnetic Resonance Imaging of the Brain and Spine, pp. 467–477. Raven Press (1991)
2. Edelman, R.R., Hesselink, J.R.: Clinical Magnetic Resonance Imaging. W.B. Saunders Company, Philadelphia (1990)
3. McDonald, W.I., Compston, A., Edan, G., Goodkin, D., Hartung, H.P., Lublin, F.D., McFarland, H.F., Paty, D.W., Polman, C.H., Reingold, S.C., Sandberg-Wollheim, M., Sibley, W., Thompson, A., van den Noort, S., Weinshenker, B.Y., Wolinsky, J.S.: Recommended Diagnostic Criteria for Multiple Sclerosis: Guidelines from the International Panel on the Diagnosis of Multiple Sclerosis. Ann. Neurol. 50(1), 121–127 (2001)
4. Tintoré, M., Rovira, A., Río, J., Nos, C., Grivé, E., Sastre-Garriga, J., Pericot, I., Sánchez, E., Comabella, M., Montalban, X.: New Diagnostic Criteria for Multiple Sclerosis: Application in first Demyelinating Episode. Neurology 60(1), 27–30 (2003)
5. Miller, D.H., Barkhof, F., Frank, J.A., Parker, G.J.M., Thompson, A.J.: Measurement of Atrophy in Multiple Sclerosis: Pathological Basis, Methodological Aspects and Clinical Relevance. Brain 125(8), 1676–1695 (2002)
6. Boesen, K., Rehm, K., Schaper, K., Stoltzner, S., Woods, R., Lüders, E., Rottenberg, D.: Quantitative comparison of four brain extraction algorithms. Neuroimage 22(3), 1255–1261 (2004)
7. Lemieux, L., Hammers, A., Mackinnon, T., Liu, R.S.N.: Automatic Segmentation of the Brain and Intracranial Cerebrospinal Fluid in T1-weighted Volume MRI Scans of the Head, and its Application to Serial Cerebral and Intracranial Volumetry. Magn. Reson. Med. 49(5), 872–884 (2003)
8. Anbeek, P., Vincken, K.L., van Bochove, G.S., van Osch, M.J.P., van der Grond, J.: Probabilistic Segmentation of Brain tissue in MR imaging. Neuroimage 27(4), 795–804 (2005)
9. Sastre-Garriga, J., Ingle, G.T., Chard, D.T., Cercignani, M., Ramió-Torrentà, L., Miller, D.H., Thompson, A.J.: Grey and White Matter Volume Changes in Early Primary Progressive Multiple Sclerosis: a Longitudinal Study. Brain 128(6), 1454–1460 (2005)
10. Datta, S., Sajja, B.R., He, R., Wolinsky, J.S., Gupta, R.K., Narayana, P.A.: Segmentation and Quantification of Black Holes in Multiple Sclerosis. Neuroimage 29(2), 467–474 (2006)
11. Sharma, J., Sanfilipo, M.P., Benedict, R.H.B., Weinstock-Guttman, B., Munschauer, F.E., Bakshi, R.: Whole-Brain Atrophy in Multiple Sclerosis Measured by Automated versus Semiautomated MR Imaging Segmentation. AJNR 25(6), 985–996 (2004)
12. Aymerich, F.X., Montseny, E., Sobrevilla, P., Rovira, A.: FLCSFD- a Fuzzy Local-Based Approach for Detecting Cerebrospinal Fluid Regions in Presence of MS Lesions. In: ICME International Conference on Complex Medical Engineering, pp. 1–6 (2009)
13. Aymerich, F.X., Sobrevilla, P., Montseny, E., Rovira, A., Gili, J.: Automatic Segmentation of Intracraneal Region from Magnetic Resonance Images. Magnetic Resonance in Physics, Biology and Medicine 11(S1), 141 (2000)
14. Yager, R.R.: Families of OWA Operators. Fuzzy Sets and Systems 59, 125–148 (1993)
15. Plummer, D.L.: Dispimage: a Display and Analysis Tool for Medical Images. Riv. Neuroradiol. 19, 1715–1720 (1992)